Chemistry of OH and HO_2 radicals observed at Rishiri Island, Japan, in September 2003: Missing daytime sink of HO_2 and positive nighttime correlations with monoterpenes

Yugo Kanaya*,[1] Renqiu Cao,[1] Shungo Kato,[2] Yuko Miyakawa,[2] Yoshizumi Kajii,[2] Hiroshi Tanimoto,[3] Yoko Yokouchi,[3] Michihiro Mochida,[4,5] Kimitaka Kawamura,[4] Hajime Akimoto[1]

[1]Frontier Research Center for Global Change, Japan Agency for Marine-Earth Science and Technology, 3173-25 Showa-machi, Kanazawa-ku, Yokohama, Kanagawa 236-0001, Japan.

[2]Tokyo Metropolitan University, Hachioji, Japan.

[3]National Institute for Environmental Studies, Tsukuba, Japan.

[4]Institute of Low Temperature Science, Hokkaido University, Sapporo, Japan.

[5]Now at Institute for Advanced Research, Nagoya University, Nagoya, Japan.

*Correspondence to: Y. Kanaya (yugo@jamstec.go.jp)

Abstract. We used laser-induced fluorescence to measure concentrations of OH and HO_2 at Rishiri Island, Japan, during September 2003. The average maximum daytime concentrations were 2.7×10^6 cm^{-3} for OH and 5.9 pptv for HO_2. The observed concentrations were compared to those predicted by a photochemical box model constrained by ancillary observations. During the daytime, the model overestimated HO_2 levels

by an average of 89% and OH levels by an average of 35%. This overestimate of OH was rectified when the model was constrained by observed HO_2 levels, suggesting that loss processes of HO_2 were missing in the model. We calculated the loss rates of HO_2 required to bring the modeled HO_2 levels into agreement with observed levels. We then studied processes that are capable of explaining the loss rates, including halogen chemistry, heterogeneous loss of HO_2 on aerosol surfaces, and the possibility of more rapid HO_2 + RO_2 reactions than expected. In the nighttime, most of the observed hourly-averaged OH and 10-min-averaged HO_2 concentrations were statistically significant, and fell in the ranges (0.7–5.5)x10^5 cm^{-3} and 0.5–4.9 pptv, respectively. Both HO_2 and OH concentrations showed strong positive correlations with total monoterpene concentrations, strongly suggesting that the radicals were produced via reactions of monoterpenes. The median nighttime modeled-to-observed ratios were 1.29 and 0.56 for HO_2 and OH, respectively. These ratios dropped to 0.49 and 0.29 during the evening of 25 September, possibly related to the presence of unmeasured olefinic species or chemical reactions involving RO_2 that are poorly represented in the model.

Index terms: 0365 Atmospheric Composition and Structure: Troposphere composition and chemistry;

0368 Atmospheric Composition and Structure: Constituent transport and chemistry;

0322 Atmospheric Composition and Structure: Constituent sources and sinks;

0315 Atmospheric Composition and Structure: Biosphere/atmosphere interactions;

Keywords: hydroxyl radical, hydroperoxy radical, model comparison, monoterpene, tropospheric chemistry

1. Introduction

Technological advances over the past two decades have enabled the accurate measurement of ultra-low concentrations of OH, HO_2, and RO_2 radicals present in the troposphere [e.g., *Heard and Pilling*, 2003]. These radicals have been observed during a number of intensive ground-level field campaigns that enable the classification of observations into various environmental subcategories such as urban, coastal/open ocean, and forest. The behavior of the radicals has been studied during field campaigns in each of these subcategories, making it easier to determine previously unidentified processes, if present, for each type of atmosphere. The daytime and nighttime behavior of the radicals can be discussed separately, as their production processes are expected to be totally different during the day and night.

Several studies undertaken at pollution-free coastal sites have found that the daytime behavior of OH and HO_2 radicals is different from that expected for conventional tropospheric chemistry mechanisms. Modeled HO_2 concentrations exceeded observed values by 70% for a study at Rishiri island (Japan) in June 2000 [*Kanaya et al.*, 2002a], by 40% for a study at Cape Grim (Australia) in February 1999 [*Sommariva et al.*, 2004], and by 260% and 100% for studies at Mace Head (Ireland) in May 1997 and August/September 2002 [*Carslaw et al.*, 2002; *Sommariva et al.*, 2006]. These values suggest that a loss process of HO_2, outside the scope of our current understanding, is responsible for differences between predicted and observed values. The overestimation at Rishiri Island is possibly related to the perturbation of HO_x (OH and HO_2) radical chemistry by iodine chemistry, as several organoiodines were detected at the site in June 2001 [*Kanaya et al.*, 2002a]. IO and BrO radicals, if present in the atmosphere, would potentially react with HO_2

at significant rates, although they were not directly measured at the site during the study period.

For the study at Mace Head, inorganic halogenated species such as I_2, IO, and/or BrO were detected, providing strong evidence of the perturbation of HO_x chemistry by halogen chemistry [*Sommariva et al.*, 2006; *Bloss et al.*, 2005]. Although our knowledge of the missing loss process of HO_2 at coastal sites has gradually improved, we are yet to determine the geographical extent of those regions where halogen chemistry influences HO_x chemistry or the nature of seasonal changes in this influence. No clear trends have been reported for OH concentrations: *Kanaya et al.* [2002a] reported that their model underestimated OH levels by 36% at Rishiri Island, whereas *Sommariva et al.* [2004] documented that their model overestimated OH levels by 10–20% at Cape Grim, and the model used by *Sommariva et al.* [2006] was able to reproduce OH levels to within 25% of observed levels at Mace Head in 2002. *Carslaw et al*. [2002] overestimated OH levels at Mace Head by 140% in 1997. Clearly, additional field campaigns are needed to fully characterize the behavior of OH and HO_2 in the coastal atmosphere.

Nighttime measurements of radical concentrations are technically challenging because the concentration levels are close to the detection limits of measuring instruments; consequently, a special care is necessary to take measurements that are free from chemical interference. From a scientific perspective, nighttime concentration levels at forested sites deserve special attention because the production of OH, HO_2, and RO_2 radicals is promoted by rapid O_3/NO_3 reactions with biogenic hydrocarbons that contain double bonds in their molecular structures. It is known that monoterpenes ($C_{10}H_{16}$) can be emitted from vegetation to the atmosphere at significant rates, even at nighttime, and these emissions readily accumulate in the shallow

and stable nocturnal boundary layer. Reactions of the monoterpenes with O_3 and NO_3 potentially result in the formation of OH, HO_2, and RO_2 radicals. Despite the current level of qualitative knowledge concerning radical production, quantitative characterization of radical concentrations and their nighttime production rates have been performed less frequently than investigations of daytime rates, for which the radical concentrations are quantitatively characterized as functions of $J(O^1D)$ values and NO_x concentrations.

Previous studies have compared observed nighttime concentrations of radicals under forested conditions with modeled concentrations. During PROPHET campaigns performed at a forested tower site in the vicinity of the University of Michigan Biological Station during the summer of 1998, OH and HO_2 concentrations were measured using laser-induced fluorescence (LIF). Typical overnight levels of OH were $1.1x10^6$ cm^{-3} (0.04 pptv), while levels of HO_2 ranged from 1 to 4 pptv [*Faloona et al.*, 2001]. Among the measured monoterpene species, α-pinene and β-pinene were dominant, with median overnight mixing ratios of 13 and 26 pptv, respectively. Although their ozonolysis reactions were considered to be the most important processes leading to radical production, the amount of monoterpene was insufficient to explain the nighttime OH levels predicted by the model [*Faloona et al.*, 2001]. Accordingly, the presence of unmeasured and highly reactive biogenic terpenoids was hypothesized, whose fast ozonolysis reaction rates might have explained the OH levels; however, this hypothesis resulted in higher-than-measured HO_2 levels. During a further field campaign at the same site during the summer of 2001, nighttime OH concentrations were typically found to be below the detection limit ($3x10^5$ cm^{-3}) of the measuring instrument, one based on chemical ionization mass spectrometry (CIMS) [*Tanner et al.*, 2002]. Consequently, the experiment was

unable to reproduce the results of the study undertaken in 1998.

At Rishiri Island, nighttime HO_2 levels were 1–5.5 pptv in June 2000, with elevated concentrations of monoterpenes (summed concentrations were >1 ppbv at times) that were presumably emitted from coniferous forests located at the slope of a mountain in the center of the island [*Kanaya et al.*, 2002b]. The dominant monoterpene species were camphene, α-pinene, β-pinene, and limonene. The results showed a weak positive correlation between observed HO_2 and monoterpene concentrations (n = 21, R^2 = 0.37); however, simultaneous measurements of HO_2 and monoterpene were only made at hourly intervals, limited by the measurement cycle of the on-site gas chromatograph. This low density of sampling prevents a more detailed analysis of the relationship between HO_2 and monoterpene.

In September of 2003 we conducted another intensive field campaign at Rishiri Island, with a focus on studying OH and HO_2 chemistry under daytime coastal conditions and nighttime forest-like conditions. Both of the conditions were expected from changes in the airmass over the site associated with land–sea breezes. In this campaign, precise measurements were made of the concentrations of OH and HO_2 radicals using an improved LIF instrument, accompanied by simultaneous measurements of a full suite of chemical species and parameters. Continuous measurements of total monoterpene concentrations were performed via proton-transfer reaction-mass spectrometry (PTR-MS) to provide an improved analysis of nighttime chemistry.

The above observations are described in Section 2, and the box model used to predict OH and HO_2 levels is outlined in Section 3. Observed OH and HO_2 data are presented in the first part of Section 4 followed by

a qualitative analysis of these data and separate comparisons with daytime and nighttime model predictions. The model systematically overestimates daytime HO_2 and OH levels. The required loss rates for HO_2 to bring the modeled levels into agreement with observations are then calculated, and we consider a number of processes that might explain these values. A strong positive correlation is observed between nighttime OH/HO_2 and monoterpene concentrations. Observed nighttime OH and HO_2 concentrations are then compared with modeled concentrations.

2. Observations

2.1. Site description

The intensive field campaign took place on Rishiri Island, north Japan, a small circular island with a diameter of ~15 km. The observatory (45.07°N, 141.12°E, 35 m asl) is located in the south of the island, approximately 800 m from the nearest coastline to the south [*Kanaya et al.*, 2002a]. A mountain (1721 m elevation) is located in the center of the island, to the north of the study site. Backward trajectory analyses show that non-polluted airmasses generally arrive at the site from east Siberia, although polluted airmasses were recorded on several days, presumably polluted by emissions from Chinese cities and nearby cities in Japan (Sapporo, with a population of 1.8 million, is 220 km from the study site, and Wakkanai, with a population of 40,000, is 50 km from the site). Local pollution derived from the island itself can be disregarded. The median daytime (0900–1500 LST (local standard time: UT+9 h) O_3, CO, NO, and NO_2 concentrations were 31 ppbv, 141 ppbv, 74 pptv, and 208 pptv, respectively.

It was typically the case that a land–sea breeze developed over the island. During the daytime, the local wind direction at the observatory was typically from the south, bringing a marine airmass to the site. In the nighttime, however, the typical wind direction was from the north and the wind speed was relatively low, enhancing the effect of monoterpenes emitted from coniferous forests (e.g., *Picea jezoensis*) located close to the observatory.

2.2. Observed species and parameters

The chemical species and parameters measured during the intensive measurement period (12–28 September, 2003) are listed in Table 1. They included OH/HO_2, CO, NMHCs, OVOCs, NO/NO_2, O_3, H_2O, organoiodines, aerosol particle number densities, and photolysis frequencies (*J* values) of atmospheric species. Mixing ratios of NO and NO_2 were measured using a chemiluminescence instrument equipped with a Xenon lamp as a photolytic converter (CLD770ALppt and PLC760, Eco Physics). The detection limits of NO and NO_2 were 22 and 45 pptv (signal-to-noise (S/N) ratio = 2; measurement time: 1 min), respectively. Mixing ratios of O_3 and CO were monitored using conventional instruments based on photo-absorption in the UV and infrared wavelength regions, respectively. The observations of other species important to the analysis in this paper are described in detail in the following subsections.

2.2.1. Hydrocarbon and halocarbon measurements

Whole-air sampling using Silco-steel canisters (Restek) was conducted on 42 occasions during the

campaign. The sampled air was analyzed following the campaign using GC-FID and GC-MS systems coupled with pre-concentration [*Kato et al.*, 2004]. The observed species were ethylene, acetylene, ethane, propylene, propane, CH_3Cl, iso-butane, 1-3-butadiene, n-butane, trans-2-butene, CH_3Br, cis-2-butene, 3-methyl-1-butene, iso-pentane, n-pentane, isoprene, DMS, n-hexane, benzene, heptane, toluene, octane, ethylbenzene, m-/p-xylene, o-xylene, α-pinene, camphene, β-pinene, limonene, CCl_2F_2, $C_2Cl_2F_4$, CCl_3F, CH_2Cl_2, $CClF_2CCl_2F$, $CHCl_3$, $C_2H_4Cl_2$, and CCl_2CCl_2. Speciation of monoterpenes and the determination of their concentrations were conducted using two GC-based instruments. No monoterpene species other than the four species listed above (α-pinene, camphene, β-pinene, and limonene) were identified.

A PTR-MS instrument was used with the selected ion mode with a measurement cycle of 20 s, consisting of 1-s measurements with masses of 31, 33, 42, 45, 59, 63, 69, 71, 79, 93, 107, 121, and 137 [*Kato et al.*, 2004]. Ten-minute averaged signals with a mass of 137 ($C_{10}H_{17}^+$) were used to determine total monoterpene concentrations. Measurement of the zero level was periodically undertaken by introducing zero air into the instrument for 15 min every hour; the zero air was produced by passing ambient air through a heated Pt catalyst. It is known that monoterpenes make fragmentation peaks, especially at a mass of 81, but these fragmentation peaks were not monitored. The calibration factor of the instrument, in terms of total monoterpene, was determined to ensure that the total concentration was in agreement with the summed concentration of the four monoterpene species measured by GC-MS. The sensitivity of the GC-MS was in turn calibrated to the concentrations derived from GC-FID, whose sensitivity to monotepenes was estimated from a linear regression between carbon numbers of more than 50 hydrocarbon species in a

standard gas mixture and their sensitivities. The detection limit of monoterpene concentrations measured using PTR-MS was estimated to be 20 pptv.

Another series of 30 canister samples was collected at the observatory and at a coastal site during the campaign to enable an analysis of CH_3Cl, CH_3Br, CH_3I, C_2H_5I, CH_2Br_2, $CHBr_2Cl$, $CHBr_3$, CH_2ClI, CH_2I_2, CH_2BrI, and DMS using GC-MS [*Yokouchi et al.*, 2005].

2.2.2. OH and HO_2 measurements

Although based on the instrument used by *Kanaya et al.* [2001], the LIF instrument used to measure OH and HO_2 in the present study was improved prior to the campaign. Briefly, the instrument employed a new Q-switched YAG laser operated at a repetition rate of 8 kHz (QDP-100-532QS-MM, Quantronix) to pump a dye laser; this was installed in place of the 1 kHz laser used previously. The dynode-gated photomultiplier that had been used previously to detect OH fluorescence was replaced with a gated channel photomultiplier. The increase in the laser repetition rate and the reduction in the afterpulse rates in the fluorescence detection system [*Kanaya and Akimoto*, 2006] improved the detection limit of the instrument. The typical nighttime detection limit with an S/N ratio of 2 was estimated to be $3x10^5$ cm^{-3} as a 1-min value (with each individual 1-min measurement with the laser wavelength being turned on and off resonant to the OH absorption line) and $9x10^4$ cm^{-3} as a 1-hour value (with 23 and 7 1-min measurements with an on-and-off resonance), enabling the detection of OH under tolerable S/N ratios. An increase in the solar scattering signal resulted in an impaired daytime detection limit (~$1x10^6$ cm^{-3} for a 1-min measurement), although its

rate was measured in a second gate period between the laser pulses and subtracted from the signal measured in the main gate period immediately after the laser pulse. A single fluorescence detection cell mounted on top of a small tower (4 m) was used to sequentially measure OH and HO_x ($OH+HO_2$). During the HO_x measurement mode, NO was added to the sampled air to titrate HO_2 to OH. The air-sampling-point was located 5.4 m above ground level, higher than the canopy level of the surrounding vegetation (typically <3 m).

A test conducted prior to the campaign showed that the instrument had a small positive sensitivity to atmospheric ozone. The OH level equivalent to the interference was parameterized using the formula:

$$[OH]_{eq.}\ (cm^{-3}) = (1800+46 \times P\ (mW)) \times [O_3\ (ppbv)], \quad (1)$$

where P is the laser power in mW. The equivalent OH level was typically 6×10^4 cm^{-3} with 11 mW laser power and an ozone mixing ratio of 25 ppbv, constituting a small yet significant fraction of the raw nighttime OH signal. The raw nighttime hourly OH signal showed a weak negative dependence on ozone concentration (R^2 = 0.03), suggesting that ozone interference was not the primary component of the nighttime OH signal. The test experiment with ozone that was conducted prior to the campaign did not show a clear dependence of the signal on H_2O mixing ratios of 1–1.5 %v/v, the typical range at Rishiri during the campaign. The independence of H_2O and the laser-power-independent term in equation (1) suggest the possibility that the interference arose from processes other than $O(^1D) + H_2O$; for example, reactions at wall or those with VOCs. The nighttime OH levels presented in the following sections are those obtained after subtraction of the equivalent level of OH signals associated with ozone interference.

The OH and HO_2 signal levels for times that zero air was introduced into the instrument were measured on 10 different days during the campaign, yielding average values of -1.9×10^4 cm^{-3} and 3.1×10^6 cm^{-3} (0.13 pptv), respectively. While the OH level with zero air was statistically insignificant and was therefore not taken into account in our analysis, the HO_2 level with zero air was likely to have been affected by impurities within the added NO flow and was therefore subtracted from all of the ambient HO_2 data prior to analysis.

The LIF instrument was calibrated by producing OH and HO_2 from the simultaneous photolysis of O_2 and H_2O at 185 nm [*Kanaya et al.*, 2001] on 13 different days. The day-to-day fluctuation of the calibration factor was only ±12% (1σ). The conversion efficiency of HO_2 to OH was measured during calibrations [*Kanaya et al*., 2001]. The efficiency was also stable, being 85 ± 5 (1σ) %. Systematic uncertainties in the OH and HO_2 calibration, which mainly reflected uncertainty in the ozone concentration produced in the calibrator, were estimated to be ±20% and ±22% (1σ), respectively. The precision of hourly-averaged OH was estimated to be 6×10^4 cm^{-3} (1σ).

2.2.3. Measurements of *J* values

Downwelling solar spectral actinic flux was measured using a spectroradiometer in the wavelength 280–700 nm with a resolution of 1.8 nm. The observed actinic flux was convoluted with the absorption cross-section and the photodissociation quantum yield of each molecule to calculate *J* values (photolysis frequencies) for NO_2, O_3 (to produce $O(^1D)$), HONO, HCHO, CH_3CHO, CH_3OOH, H_2O_2, CH_2I_2, I_2, and

HOI. The observed $J(O^1D)$ and $J(CH_3CHO)$ values contained large uncertainties due to a stray light problem in the spectroradiometer [*Kanaya et al.*, 2003]. Accordingly, these two *J* values were estimated by multiplying transmission factors, calculated as ratios of observed $J(NO_2)$ to clear-sky $J(NO_2)$, with the clear-sky $J(O^1D)$ and $J(CH_3CHO)$ values calculated using the radiative transfer model TUV version 4.1 [*Madronich and Flocke*, 1998]. The transmission factors were not strongly dependent on the wavelength when solar zenith angle was <60° [*Kanaya et al*., 2003]. The downwelling components of *J* values were multiplied by a factor of 1.1 to account for their upwelling components and were used as input parameters in the model calculations.

2.2.4. Size distribution of aerosol particles

Number densities of aerosol particles were measured as a function of size using a scanning mobility particle sizer (model 3936, TSI) with a size range of 4.5–163 nm and using an optical particle counter (KC18, Rion) with size bins of >0.1, >0.15, >0.2, >0.3, and >0.5 μm. The observed size distribution of the aerosol particles was then used to calculate the heterogeneous loss frequency k_γ of atmospheric molecules on aerosol surfaces, as determined by the following Fuchs–Sutugin equation:

$$k_\gamma = \int \frac{4\pi D r}{1 + K_n\left(\frac{1.333 + 0.71K_n^{-1}}{1 + K_n^{-1}} + \frac{4(1-\gamma)}{3\gamma}\right)} N dr \ , \qquad (2)$$

where *Kn* is the Knudsen number, *r* is the radius of the aerosol, and *N* is the number density of the particles. The gas phase diffusion coefficient (*D*) of gaseous molecules was assumed to be 0.247 $cm^2\ s^{-1}$

[*Mozurkewich et al.*, 1987].

3. Model calculations

Our box model used to predict OH and HO_2 levels was based on the Regional Atmospheric Chemistry Mechanism (RACM) [*Stockwell et al.*, 1997], but was expanded to include monoterpene chemistry as described by *Kanaya et al.* [2002b]. The rate coefficients of the OH + NO_2 and $O(^1D)$ + N_2 reactions were updated as suggested by *Sander et al.* [2003] and *Ravishankara et al.* [2002], respectively. In the base run, neither heterogeneous loss of HO_2 on aerosol surfaces nor halogen chemistry was taken into account. The model calculation was conducted by constraining the concentrations of O_3, H_2O, CO, NO_x, SO_2, and hydrocarbons and *J* values to the observed values. The concentrations of ethane, acetylene, propane, isobutene, n-butane, i-pentane, n-pentane, n-hexane, and benzene were estimated from linear regression lines with respect to CO (R^2 ranged between 0.04 and 0.41). All 10-min averages of isoprene and total monoterpene concentrations were derived from PTR-MS. As shown in Section 4.2.1 below, monoterpenes were assumed to consist of 28% α-pinene, 20% β-pinene, 37% camphene, and 15% limonene. Concentrations of other minor hydrocarbons were assumed to be the average values determined during the campaign. The average diurnal variations in the concentrations of HCHO and acetaldehyde as measured during the previous campaign at the same site in June 2000 were halved and were used as constraints for the concentrations of HCHO and ALD (a category of RACM for acetaldehyde and higher aldehydes) in the model runs. A three-dimensional photochemical model predicted that concentrations of HCHO at the site in

September are nearly half levels of those in June [*Tanimoto et al.*, 2002]. The assumed midday peak and nighttime minimum concentrations of HCHO were 386 and 145 pptv. Sensitivity studies indicate that the predicted OH and HO_2 levels were almost insensitive to HCHO and ALD concentrations; median changes in the daytime (0900–1500 LST) OH and HO_2 levels were only <1% and <11% even when HCHO and ALD concentrations were doubled (increased to the levels of June 2000) or were further reduced by a factor of 2 from those in the base run. The boundary layer height (*BLH*) was assumed to be 200 m in the night and 1000 m in the daytime. The deposition velocities (v_d) of H_2O_2, organic peroxides, HNO_3, carbonyls, organic nitrates, and PANs were assumed to be 1, 0.5, 2, 1, 1, and 0.2 cm s^{-1}, respectively [*Brasseur et al.*, 1998]. An uncertainty in deposition terms, calculated as $-v_d/BLH$, of a factor of 2 was propagated to the uncertainties in OH and HO_2 levels of only <5%. A time-dependent approach was used to simulate diurnal variations in the concentrations of radicals on each day during the period 18–28 September. The time of 0000 LST on each day was regarded as the initial time, and an integration over 24 hours was conducted by regarding 10-min data as segments of the 24-hour period. This integration was repeated four times to stabilize the concentrations of unconstrained species (e.g., unmeasured carbonyl species). The results for the last 24 hours were used as output for each day.

To predict OH and HO_2 concentrations for the three nights (21–22, 25–26, and 27–28 September) when OH and HO_2 were continuously measured, model calculations were conducted in the same manner as that described above but with initialization at 1200 LST on the first day. On the basis of Monte-Carlo simulations, the 1-σ uncertainties of the predicted OH and HO_2 levels were estimated to be ±28% and

±24% (1σ) for OH and HO_2 in the daytime, respectively, and ±31% and ±34% in the nighttime. The 1-σ uncertainties taken into account in the Monte-Carlo run are provided as auxiliary material.[1]

To predict HO_2 and OH, two further model runs were conducted with OH or HO_2 concentrations constrained to the observed levels, respectively. We performed three more sets of model runs for the daytime, each with heterogeneous loss of HO_2, with iodine chemistry and with larger rate coefficients for the HO_2+RO_2 reactions (see Subsection 4.1.2). The iodine chemistry added to the model was based on *Kanaya et al.* [2002a], although revised with new kinetic data compiled by *Sander et al.* [2003]. When necessary, the heterogeneous chemistry of HO_2 and iodine species was considered by adding the following reaction steps, with frequencies k_γ, as calculated from Eq. (2):

$$HO_2 + \text{aerosol} \rightarrow \text{no products in gas phase} \quad (3)$$

$$\text{iodine species} + \text{aerosol} \rightarrow \text{I in the gas phase} \quad (4)$$

It was assumed that all the iodine atoms within the molecules that underwent the heterogeneous process were recycled back to the gas phase as iodine atoms. Other model studies employ a lower yield of iodine atoms [e.g., *Vogt et al.*, 1999]. The choice of the yield is not important in this study, where we only estimate IO levels required to reduce HO_2 to the observed levels and do not examine partitioning among the inorganic iodine species.

4. Observed and calculated OH and HO_2 concentrations

Figure 1 shows the observed OH and HO_2 concentrations for the period 18–28 September 2003. All the

plotted data points are 10-min averages. Both the observed OH and HO_2 concentrations show clear diurnal variations, with daytime maxima of 4–8 pptv for HO_2 and (1–6)x10^6 cm^{-3} for OH. The hourly-averaged diurnal variations are shown in Figure 2. The daytime maximum of OH and HO_2 occurred during 11*H* (the hour between 1100 and 1200 LST) and 12*H* (the hour between 1200 and 1300 LST), respectively. The averages of the maxima were 2.7x10^6 cm^{-3} for OH and 5.9 pptv for HO_2. In the nighttime, most of the observed hourly-averaged OH and 10-min-averaged HO_2 concentrations were statistically significant, with observed ranges of (0.7–5.5)x10^5 cm^{-3} and 0.5–4.9 pptv, respectively. The OH and HO_2 concentrations modeled using RACM (with expanded monoterpene chemistry) are also shown in Figure 1 (gray lines). Detailed comparisons between observed and modeled OH and HO_2 are provided separately in the following subsections for daytime and nighttime values.

4.1. Analysis of observed and calculated values of daytime OH and HO_2

It is evident from Figure 1 that the model significantly overestimated the daytime HO_2 and OH concentration levels, although the day-to-day patterns of variations in OH were well captured by the model. The scatterplots (Figure 3) of observed and calculated OH and HO_2 for the 6-hour period about midday (0900–1500 LST) show that the model overestimated HO_2 levels by an average of 89% and OH levels by an average of 35%. The discrepancy in the HO_2 levels cannot be explained by uncertainties in the observation data and model calculation, although the discrepancies in OH levels were within the combined uncertainties. It should also be noted that the model's overestimation of OH was remedied when the model

was constrained by the measured levels of HO_2 (Figure 1); the observed OH levels are consistent with the observed HO_2 levels, rather than the modeled HO_2. It is difficult to explain the overestimation of daytime HO_2 levels only by the overestimation of the radical production rate; in an additional model run with the radical production rate reduced to the limit of uncertainty, where concentrations of ozone, H_2O, and aldehydes and $J(O^1D)$ values were simultaneously reduced by factors of 1.2, 1.1, 2.0, and 1.3, respectively, midday HO_2 levels were reduced only by 25% in average. On the basis of these analyses, it is reasonably suggested that loss processes for HO_2 are missing from our current understanding of tropospheric chemistry.

The same analysis undertaken for the same site in June 2000 showed that the model overestimated midday HO_2 levels by 70% and underestimated OH levels by 36% [*Kanaya et al.*, 2002a]. The daytime (0900–1500 LST) median NO concentration was similar (83 pptv in June 2000 and 74 pptv in September 2003), while the median radical production rate in June 2000 (5.3×10^6 radicals cm^{-3} s^{-1}) was higher than that in September 2003 (2.1×10^6 radicals cm^{-3} s^{-1}). The degree of overestimation of HO_2 was similar for the two periods, raising the possibility that a common process was responsible for the differences. In contrast, the magnitude relation between the modeled and observed OH levels for the two periods was opposite. This finding suggests that the fate of the product of the missing HO_2 reaction, even if commonly present, was different between the two periods with respect to the generation of OH. It should also be noted that OH measurements in June 2000 were associated with large uncertainties because of a worse detection limit.

In Figure 4, the modeled-to-observed ratios for OH and HO_2 are plotted against the NO mixing ratio. The

overestimation of HO_2 was significant for low NO concentrations, as found in our previous study conducted during June 2000. The OH ratio was nearly constant over the NO range between 10 and 1000 pptv; this differs from the case for June 2000 where the OH ratio was significantly lower than unity for low NO mixing ratios (10–50 pptv) [*Kanaya et al.*, 2002a].

5

4.1.1. Required loss rate of HO_2

An imaginary loss process of HO_2, producing no products in the gas phase, was added to the model to calculate the frequency *k* required to reduce the modeled HO_2 levels to the measured levels for the 10-min data:

10 $$HO_2 + X \rightarrow \text{ no products; } k\ (s^{-1}) \quad (5)$$

The HO_2 concentration in the model steadily decreased with increasing *k*. Technically, the *k* value was optimized such that the modeled HO_2 agreed with the observed HO_2 to within 1%. Temporal variations in calculated values of *k* are shown in Figure 5. The rate showed midday maxima in the range of 0.01–0.02 s^{-1}, reflecting the fact that the discrepancy in HO_2 levels was greatest at midday. The same analysis was 15 undertaken for the data set collected in June 2000. The composite diurnal variations in *k* for the two campaigns are compared in Figure 6. The daytime *k* for the two campaigns is surprisingly similar, at approximately 0.015 s^{-1}. The earlier increase and later decrease in *k* recorded in June 2000 compared with the present study could reflect the earlier sunrise and later sunset times of the 2000 study.

4.1.2. Possible explanations of the loss rate

Here we consider those processes that are able to explain the calculated *k* range and its temporal variations during September 2003. First, we calculated correlation coefficients between calculated *k* and all the observed and calculated concentrations of chemical species, aerosol number density, and meteorological parameters, even including tidal height, transmission factor of $J(NO_2)$, wind direction/speed, and *J* values. The selected factors that showed high correlation coefficients with *k* are listed in Table 2; these factors might be involved in or related to the important missing process of HO_2. Using this analysis as a guide, three potentially important factors (halogen chemistry, heterogeneous loss of HO_2 on aerosol surfaces, and HO_2 + RO_2 reactions that occurred faster than expected) were chosen for further consideration. As any single hypothesis does not appear to fully explain our observations, a combination of factors is the most likely explanation for the low levels of observed daytime HO_2.

4.1.2.1. Halogen chemistry

If present in the atmosphere, halogen monoxides such as BrO and IO react rapidly with HO_2 to form HOBr or HOI. Photolysis of the produced HOBr or HOI then releases OH to the atmosphere [*Davis et al.*, 1996; *Stutz et al.*, 1999]. In contrast, the heterogeneous loss of HOBr and HOI would result in a loss of HO_x from the atmosphere [*Kanaya et al.*, 2002a; *Bloss et al.*, 2005].

The photolysis of halocarbons is one of the important processes in terms of initial release of active halogen atoms and thus halogen oxides that are easily formed by the reactions of halogen atoms with ozone.

Among the detected halocarbons, CH_3I (R = 0.31) and $CHBr_3$ (R = 0.35) showed positive correlations with k (Table 2). Only those concentrations observed at 1230 and 1430 LST were used in this analysis. If multiplied by a transmission factor of $J(NO_2)$, the concentrations of CH_3I show an even higher correlation coefficient of 0.79. This analysis might therefore qualitatively indicate the possible participation of halogen chemistry in the missing chemistry.

We performed another set of model runs with the iodine chemistry mechanism to calculate the IO concentrations required to reduce HO_2 to the observed levels in a similar way to *Kanaya et al*. [2002a]. In the runs, both the photolysis of HOI and the heterogeneous loss of HOI on aerosol surfaces with an uptake coefficient of 0.5 were taken into account. The IO levels calculated in this way were in the range of 10–40 pptv for midday. This set of model runs resulted in an overestimation of the midday concentrations of OH radicals by 74%. Even in the case where the produced HOI is assumed to be lost via an unknown fast process and never recycled to atmospheric HO_x radicals, 5 pptv of IO (1.2×10^8 cm^{-3}) is required to explain an HO_2 loss rate of 0.01 s^{-1}, considering a rate coefficient of the HO_2 + IO reaction of 8.4×10^{-11} cm^3 $molecule^{-1}$ s^{-1} [*Sander et al.*, 2003]. This case defines the minimum level of IO required to explain the observed HO_2 levels.

The maximum concentrations of CH_2ICl and CH_2I_2 observed at the observatory and at a coastal site in September 2003 were 0.1 and 0.09 pptv, respectively, while a single daytime measurement of CH_2I_2 and CH_2ICl at the coastal site in June 2001 recorded values of 0.8 and 0.4 pptv, respectively. Although their photolysis can produce iodine atoms in the atmosphere relatively quickly, their levels in September 2003

were not sufficient to produce IO concentrations of 5 pptv. The maximum levels recorded in September 2003 were lower than those measured at Cape Grim (up to 0.39 pptv of CH_2ICl) [*Carpenter et al.*, 2003], where up to 0.5 pptv of IO were simultaneously detected, and Mace Head (up to 0.5 pptv of CH_2ICl and 0.45 pptv of CH_2I_2) [*Carpenter et al.*, 1999, 2000]. On the basis of these low levels of organoiodines, we were unable to obtain strong evidence of iodine chemistry at the island for the period of the present campaign. There is the alternative possibility, however, that the photolysis of other iodinated species such as I_2 is a more effective source of IO. This mechanism has recently been suggested for Mace Head [*Saiz-Lopez and Plane*, 2004]. This possibility needs to be considered further in future studies.

Bromine chemistry affects HO_2 levels in a similar way to that of iodine chemistry [*Sommariva et al.*, 2006; *Bloss et al.*, 2005]. Considering the rate coefficient of the BrO + HO_2 reaction ($2.1x10^{-11}$ cm^3 $molecule^{-1}$ s^{-1} [*Sander et al.*, 2003]), 20 pptv of BrO ($4.8x10^8$ cm^{-3}) is at least required to explain an HO_2 loss rate of 0.01 s^{-1}. The photolysis and reactions of four organobromines (CH_3Br, CH_2Br_2, $CHBr_2Cl$, and $CHBr_3$) detected at the observatory, with maximum daytime concentrations of 10.6, 1.2, 0.4, and 2.6 pptv, respectively do not adequately explain the 20 pptv of BrO. Therefore, we conclude that no strong evidence of bromine chemistry is obtained from compounds observed during the campaign, although the possibility exists that inorganic bromine species are ejected from sea-salt particles to the atmosphere upon the heterogeneous uptake of gaseous iodine species.

4.1.2.2. Heterogeneous loss of HO_2 on aerosol surfaces

Laboratory experiments [*Mozurkewich et al.*, 1987; *Hanson et al.*, 1992] and a recent molecular dynamics simulation [*Morita et al.*, 2004] indicate that the mass accommodation coefficient (α) of HO_2 can be high around unity on aqueous particles. Chemical reactions within submicron aerosols are the rate-determining steps in defining the γ of HO_2, as reported over a wide range from ~0.01 for solid surfaces [*Gershenzon et al*., 1995] to 0.5 for NH_4HSO_4 aerosols doped with copper ions [*Mozurkewich et al.*, 1987]. In several field studies, heterogeneous loss has been examined as one of the likely mechanisms leading to lower HO_2 levels at coastal sites [*Sommariva et al*., 2004, 2006; *Haggerstone et al*., 2005]. As shown in Table 2, the required loss rate shows weak positive correlations with H_2O and the particle number density within the size range 300–500 nm; this might indicate interaction between HO_2 and aqueous aerosol particles. We tested this hypothesis using the full size distribution of aerosol particles observed with a scanning mobility particle sizer and an optical particle counter, assuming $\gamma = 1$, to estimate the potential maximum influence of the process. The calculated heterogeneous loss rate of HO_2 ranged between 0 and 0.015 s^{-1} (gray line in Figure 5), similar to that of the required loss rate *k*. However, the diurnal pattern of the missing loss rate was not reproduced unless γ was assumed to change diurnally.

Another set of model runs with the heterogeneous loss of HO_2 on the aerosol surface (assuming $\gamma = 1$) was performed on the basis of reaction (3) shown above. The disparity between the observed and calculated HO_2 levels was approximately halved in this model run (red lines in Figure 1). The model runs overestimated the daytime OH levels only by 3%. Laboratory measurements of γ for aerosol particles of different compositions and surface conditions are needed to clarify the importance of the heterogeneous

process.

4.1.2.3. Reaction rate coefficients of HO_2 + RO_2

It is known that the recombination reaction of HO_2 is accelerated by the presence of H_2O, presumably due to the formation of the water complex of HO_2, HO_2–H_2O [*Sander et al.*, 2003]. The HO_2 + RO_2 reactions, which take place with a similar reaction mechanism, might be faster under humid conditions than under the dry conditions in which past kinetic experiments were performed. The RO_2 radical is a class of species that shows strong positive correlations with the missing loss rate of HO_2 (Table 2), implying their possible participation in the missing chemistry. The weak positive correlation between H_2O and the missing loss rate of HO_2 is also consistent with this possibility. A sensitivity run with rate coefficients for all the HO_2 + RO_2 reactions increased by a factor of 5 (blue lines in Figure 1) resulted in HO_2 levels similar to the case with a heterogeneous loss of HO_2. The model runs overestimated the daytime OH levels only by 5%. However, the assumption also resulted in a significant underestimation of nighttime HO_2 levels.

4.1.3. Budget of daytime radicals

The median budgets of OH and HO_2 radicals in the daytime (0900–1500 LST) are shown in Figure 7 for the base run. OH production was dominated by the $O(^1D)$ + H_2O (25%) and HO_2 + NO (66%) reactions. OH was lost mainly via reactions with CO (44%), CH_4 (14%), and isoprene (8%). HO_2 was lost via a reaction with NO (55%). The budget of the radical group (OH+HO_2+RO_2) is also shown to enable

consideration of the initial production and ultimate loss processes of the radicals by masking interconversion among the radicals. Interconversion between HO_2 and HO_2NO_2 and between the radicals and PANs was not included in the figure. More than half (66%) of the initial production of the radicals occurred with the $O(^1D) + H_2O$ reaction. The self- and cross-reactions of peroxy radicals are important to radical sink. It should be noted that the radical budgets shown in Figure 7 are for the case where the radical concentrations are overestimated. The heterogeneous loss of HO_2 on aerosol surfaces with $\gamma = 1$, if included, contributed to radical loss by 30–40% on 18 September, when the run with the process reproduced the observed daytime HO_2 levels.

4.2. Analysis of observed and calculated nighttime OH and HO_2

Considering the times of sunset (1753–1718 LST) and sunrise (0511–0533 LST) during the campaign, nighttime is defined in the present study as the period between 1800 and 0459 LST. Correlations between the concentrations of the OH/HO_2 radical and monoterpene are presented first, followed by a discussion of comparisons between observed and modeled nighttime radical concentrations.

4.2.1. Monoterpene measurements

The monoterpene species identified using GC-FID and GC-MS were α-pinene, β-pinene, camphene, and limonene. The averaged fractions of the four monoterpenes were 0.28, 0.20, 0.37, and 0.15, respectively, which are similar to the fractions 0.25, 0.20, 0.41, and 0.13 observed at the same site in June 2000. The

fractions reflect emission ratios from coniferous forest located near the site. Figure 8 shows temporal variations in total monoterpene concentrations measured using PTR-MS (averaging intervals of 10 min and 1 hour) compared to that of the sum of the four monoterpene concentrations measured via GC-MS. The measured concentrations were high in the nighttime, sometimes exceeding 1 ppbv. It is natural that the average of the total monoterpene concentration level agrees with the summed concentration of the four monoterpenes measured by GC-MS because the sensitivity of the PTR-MS instrument is determined to fulfill this requirement. However, it is not self-evident that the patterns of temporal variations in the two sets of measurements are also in good agreement. Thus, it is reasonable as a first approximation to assume for the model calculations that at all times the total monoterpene concentrations consisted of these four species at the averaged fractions.

4.2.2. Relationship between observed HO_2 or OH and total monoterpene concentrations

Figure 9a shows all the data pairs of simultaneous nighttime measurements of total monoterpene and HO_2 concentrations with a time resolution of 10 min. The number of data pairs n is 129, which is significantly higher than the 21 pairs obtained in the analysis of our previous campaign in June 2000. The higher value of n in the present study can be attributed to the rapid and continuous measurement of monoterpene via PTR-MS. The observed 10-min-averaged nighttime HO_2 ranged between 0.5 and 4.9 pptv. There is a positive correlation between HO_2 and monoterpene concentrations, with R^2 being 0.60. The correlation is even stronger ($R^2 = 0.69$) between HO_2 and Σ[monoterpene][O_3]$\phi_{radical}$, the production rate of

radicals from ozonolysis reactions of the monoterpenes, where $\phi_{radical}$ is the total radical (OH, HO_2, and RO_2) yield from the each monoterpene + O_3 reaction (Figure 9b). The assumed values of $\phi_{radical}$ were 1.57, 1.36, 1.36, and 1.52 for the ozonolysis reactions of α-pinene, β-pinene, camphene, and limonene, respectively, as estimated from the reaction mechanism of the monoterpenes [*Kanaya et al.*, 2002b]. This improvement in correlation cannot be attributed to the relationship between HO_2 and O_3, as *in-situ* observations indicate a negative correlation between them (Figure 9c). Accordingly, the strong correlation in Figure 9b strongly suggests that the radicals were initially produced by O_3 reactions with monoterpenes. This does not necessarily indicate that NO_3 reactions were negligible, as NO_3 concentrations can show a positive correlation with O_3. However, a budget analysis (Subsection 4.2.4) indicates that the NO_3 reactions were less important in producing the radicals than the ozonolysis reactions at this site with low NO_2 concentrations. *Salisbury et al.* [2001] showed that nighttime HO_2+RO_2 concentrations at Mace Head, Ireland, as measured using a PERCA instrument in spring 1997, had a positive correlation with the total NO_3/O_3 + olefin reaction rate (R^2 = 0.54). The R^2 value of 0.69 obtained in the present study is even higher than their value.

The hourly-averaged nighttime OH levels, each of which was generally calculated as an average of 23 data points with 1-min integration, showed a positive correlation with monoterpene concentration and the radical production rate (Figure 9d and e, n = 40). Most of the hourly-averaged OH levels ranged between 0.7 and 5.5×10^5 cm^{-3}, above the detection limit for 1-hour values (see Section 2). These levels were also statistically significant against fluctuations in the hourly-averaged nighttime background signal (consisting

of laser-induced afterpulses), corresponding to OH concentration levels of 6.5, 5.6, and 4.5×10^4 cm^{-3} (S/N = 1) for the nights of 21–22, 25–26, and 27–28 September, respectively. The R^2 value for Figure 9e is 0.49, higher than that for Figure 9d (0.39), although OH showed a negative correlation with O_3 (Figure 9f). These analyses of OH again suggest that the ozonolysis reactions were important in producing the radicals.

Contrary to the findings evident in Figure 9f, *Faloona et al.* [2001] found a positive correlation between nighttime OH and O_3 concentrations ($R^2 = 0.37$) measured during the PROPHET campaign in the summer of 1998. It should also be noted that *Martinez et al.* [2003] and *Ren et al.* [2003] reported positive correlations between nighttime OH and O_3 concentrations under urban conditions. The differences between the findings of the present study and those of previous studies are attributable to the fact that ozone within the atmosphere was depleted by reactions with the monoterpenes at high concentrations or by dry deposition under calm conditions before the arrival of the air mass at the observatory from the area with emission of monoterpene in Rishiri Island.

The median of the summed monoterpene concentration measured for the PROPHET campaign was 54 pptv, lower than that in the present study. The HO_2 range recorded during the PROPHET campaign (1–4 pptv) was similar to that of the present study; however, the median OH (1.1×10^6 cm^{-3}) was higher than the OH ranges recorded in our study by more than a factor of 3. This discrepancy can be partially attributed to the higher NO_3 concentrations during the PROPHET campaign, which potentially resulted in a more rapid production of radicals. The nighttime NO_3 mixing ratio estimated for the PROPHET campaign was 2–3 pptv [*Faloona et al.*, 2001], higher than the value of 0.1–0.3 pptv estimated for the campaign at Rishiri

Island (see Subsection 4.2.4). In any case, it is clear that the nighttime OH and HO_2 levels depend on the monoterpene concentrations that define the radical production rate under forested conditions. We therefore propose that nighttime HO_x levels at forested sites need to be studied quantitatively as functions of monoterpene concentrations or the radical production rate from the reactions of monoterpenes.

5

4.2.3. Comparison with model predictions

Here we present a comparison of the observed and modeled OH and HO_2 values with a focus on the three nights (21–22, 25–26, and 27–28 September) when OH and HO_2 were measured continuously from sunset to sunrise. The averaged concentrations and meteorological parameters recorded during the three

10 nights are listed in Table 3. The average concentrations of HO_2, OH, and monoterpene were highest on the night of 25–26 September under the conditions of light wind and high relative humidity. The NO level (~5 pptv), measured as an average over each night, was statistically significant.

The observed radical concentrations are compared with modeled concentrations assuming a fixed NO mixing ratio of 5 pptv (Figure 10a–c); however, as the observed averages of NO contained high

15 uncertainties, several sensitivity runs were performed with varying NO levels between 0.1 and 50 pptv. A time-dependent positive correlation between concentrations of observed HO_2 and total monoterpene (shown as shaded bars) was again evident. The HO_2 levels modeled with NO concentrations fixed at 5 pptv (yellow lines in Figure 10) showed average values of 1.7 ± 0.2, 1.9 ± 0.3, and 1.5 ± 0.1 pptv for the three nights, respectively. The median model/observation ratio of HO_2 for the three nights was 1.29.

The model produced an overestimate on the first and third nights and an underestimate on the second night. The reasons for the overestimation might be similar to those in the daytime as studied in Subsection 4.1.2. The degree of underestimation by the model was most significant for the evening of 25 September. As shown by colored lines in Figure 10, the modeled HO_2 levels increase with increasing assumed NO levels, as NO enhances the formation of HO_2 via RO_2 + NO reactions rather than the loss of HO_2 via the HO_2 + NO reaction. The observed HO_2 concentrations on the three nights were well reproduced by model runs with NO levels of 2, 5–10, and 1 pptv, respectively. The result of the model run for 25–26 September undertaken with OH levels constrained by observations is shown by a black dashed line. In this case, NO was assumed to be 5 pptv. The high HO_2 levels (around 4 pptv) observed during the period 1800–2000 LST on 25 September was only well reproduced by this run with the OH constraint. This model run also quantitatively reproduced the decrease in HO_2 levels observed in the evening, suggesting that the observed OH levels were reasonable.

Hourly-averaged OH concentrations are compared with modeled values in Figure 10d–f. The averages of the OH levels modeled with 5 pptv of NO were (1.1 ± 0.1), (1.4 ± 0.3), and (0.9 ± 0.1)x10^5 cm^{-3} for the three nights, respectively. The median modeled-to-observed ratio of OH for the three nights was 0.56. The modeled OH concentrations increased with increasing NO, as NO promoted the production of OH via the HO_2 + NO reaction. For all three nights, the model tended to underestimate OH levels unless the NO mixing ratio was assumed to be unrealistically high (>10 pptv). The degree of underestimation by the model was most significant during 1800–2000 LST on 25 September, coincident with the underestimation

of the HO_2 level. Constraining the HO_2 concentrations to observed values did not significantly improve the agreement between modeled and observed OH levels for the three nights.

Comparisons between observed and simulated data are presented in Figure 11 as functions of the total radical production rate (in the case of OH) and its square root value (in the case of HO_2). In this analysis, modeled total radical production rates with a NO value of 5 pptv are used. The model tended to underestimate HO_2 at high values and overestimate at low values. At high values of HO_2, the modeled HO_2 mixing ratio did not increase significantly with increasing monoterpene concentration as the observed HO_2 did. This different behavior has three possible explanations. First, the production rate of the HO_2 radical could be underestimated because the $RO_2 + RO_2$ reactions are not fully represented in our reaction scheme. A sensitivity model run with a self-reaction of KETP (peroxy radicals produced by ketone oxidations), not taken into account in the mechanism, increased nighttime HO_2 levels by ~10% on 25–26 September. Secondly, it is possible that the concentration of NO, likely emitted from the soil [e.g., *Yienger and Levy*, 1995], is positively correlated with the monoterpene concentration commonly influenced by wind speed and stability of the atmosphere, thus enhancing HO_2 levels in addition to the effect of monoterpene levels as was studied in the model runs with varying NO levels. Thirdly, unmeasured highly reactive biogenic species might have been present in the atmosphere on the evening of 25 September, resulting in a production rate of HO_2 that was higher than that estimated on the basis of the identified four monoterpenes. At 1830 LST, the total concentration of the four monoterpenes measured using GC-MS (188 pptv) was lower than the total monoterpene concentration measured using PTR-MS (256 pptv), suggesting the

presence of unidentified reactive monoterpene, especially during this period. *Di Carlo et al*. [2004] implied a similar possibility of missing hydrocarbons at a forested site during nighttime.

The OH levels modeled with 5 pptv of NO showed a weaker positive dependence on the radical production rate than the observed hourly OH (Figure 11b). Although the observed OH levels were underestimated by the model at high values, some of the low values around $1x10^5$ cm^{-3} were well reproduced. Underestimation of nighttime OH concentrations by the model can be explained by the presence of unmeasured biogenic species that react rapidly with O_3 to produce OH. This is the most likely explanation for the evening of 25 September, as the HO_2 levels during this evening were well reproduced in the model run for which OH levels were constrained to observed values (see above).

4.2.4. Nighttime budget of radicals and monoterpene oxidation pathways

Figure 12 shows the production and loss processes of HO_2, OH, and the radical group ($OH+HO_2+RO_2$) as determined by the model run with a NO value of 5 pptv. It is evident that the radicals are primarily produced by the reactions of monoterpenes with O_3 rather than reactions with NO_3. The OH loss was dominated by reactions with CO, methane, and the four monoterpenes. The fact that the monoterpenes were not the most important species in terms of a reaction partner for OH indicates that unmeasured monoteprenes, if present, would readily act to increase OH production but would not largely increase the OH loss rate, resulting in higher OH concentrations at a steady state. The loss of HO_2 was governed by its reactions with O_3, NO, HO_2 itself, and RO_2. The ultimate loss processes of the radicals were dominated by

cross-reactions of the peroxy radicals.

The averages of the NO_3 levels predicted by the model calculations with 5 pptv of NO were 0.17, 0.09, and 0.27 pptv for the three analyzed nights (Table 3). The low concentrations are explained by the fact that the high monoterpene concentrations resulted in a rapid loss of NO_3. The typical loss rate of NO_3 associated with reactions with the four monoterpenes was calculated to be $1x10^{-2}$ s^{-1} on the basis of averaged monoterpene concentrations over the night of 25–26 September.

The oxidation rates of the four monoterpenes due to reactions with OH, O_3, or NO_3 were calculated as the products of the nightly-averaged concentrations of observed OH, O_3, or calculated NO_3 and the pertinent reaction rate coefficient. The lifetime of each monoterpene species was estimated as the inverse of the summed rate. The averaged lifetimes were 1.2, 3.0, 7.5, and 19 hours for limonene, α-pinene, β-pinene, and camphene, respectively. This analysis indicates that limonene and α-pinene emitted in early night, if staying in the near-ground atmosphere, do not survive through night to the morning of the following day and that the nighttime chemistry determines their initial oxidation pathways. It is interesting to note that 48% and 76% of the oxidation of β-pinene and camphene, respectively, is governed by their reactions with OH rather than those with O_3 and NO_3. Although the oxidation of α-pinene and limonene was mainly controlled by their reactions with NO_3 and O_3, oxidation by OH potentially contributes up to 30% of total oxidation.

5. Summary

The daytime HO_2 levels observed at Rishiri Island in September 2003 were overestimated by our model, as occurred in our previous campaign held at the same site in June 2000. Daytime OH levels, which were measured with higher signal-to-noise ratios in the present campaign, were also overestimated by the model. The discrepancy in OH was almost completely rectified when the model was constrained by the observed levels of HO_2. This analysis suggests the reasonableness of the observed HO_2 levels and the presence of an unknown sink of HO_2. We undertook an investigation of the possibility that iodine chemistry perturbed HO_x chemistry, but failed to uncover strong evidence of such a relationship. We also examined other possible explanations such as the heterogeneous loss of HO_2 and accelerated HO_2 + RO_2 reaction rates. A combination of these potential mechanisms is the most likely explanation for the low levels of observed daytime HO_2.

Co-located measurements of OH/HO_2 concentrations and total monoterpene concentrations using PTR-MS with high temporal resolutions revealed positive nighttime correlations between the two concentrations. The correlations were even stronger between radical concentrations and the radical production rate resulting from the reactions of O_3 with the monoterpenes. This finding strongly suggests the production of radicals from the reactions. The model simulations tended to underestimate OH and HO_2 for high values, whereas good agreement was achieved for lower values. This underestimate might have resulted from the presence of unidentified reactive monoterpene species, especially during the period 1800–2000 LST on 25 September or from RO_2 self-reactions that are not well represented in the model.

Acknowledgments. The authors are grateful to all the participants in the campaign undertaken at Rishiri Island in September 2003 for their helpful contributions. This study is supported financially by the Ministry of Education, Science, Sports, and Culture of Japan (Grants-in-aid 14780420, 15201004, and RR2002 of the Kyosei Project).

Footnote

[1]Auxiliary materials are available at ftp://ftp.agu.org/apend/jd/2006jd007987.

References

Bloss, W. J. et al. (2005), Impact of halogen monoxide chemistry upon boundary layer OH and HO_2 concentrations at a coastal site, *Geophys. Res. Lett.*, *32*, L06814, doi:10.1029/2004GL022084.

Brasseur, G. P., D. A. Hauglustaine, S. Walters, P. J. Rasch, J.-F. Müller, C. Granier, and X. X. Tie (1998), MOZART, a global chemical transport model for ozone and related chemical tracers 1. Model description, *J. Geophys. Res.*, *103*(D21), 28,265–28,290.

Carpenter, L. J., W. T. Sturges, S. A. Penkett, P. S. Liss, B. Alicke, K. Hebestreit, and U. Platt (1999), Short-lived alkyl iodides and bromides at Mace Head, Ireland: Links to biogenic sources and halogen oxide production, *J. Geophys. Res.*, *104*(D1), 1679–1690.

Carpenter, L. J., G. Malin, P. S. Liss, and F. C. Küpper (2000), Novel biogenic iodine-containing trihalomethanes and other short-lived halocarbons in the coastal East Atlantic, *Global Biogeochem. Cycles*, *14*(4), 1191–1204.

Carpenter, L. J., P. S. Liss, and S. A. Penkett (2003), Marine organohalogens in the atmosphere over the Atlantic and Southern Oceans, *J. Geophys. Res.*, *108*(D9), 4256, doi:10.1029/2002JD002769.

Carslaw, N. et al. (2002), Eastern Atlantic Spring Experiment 1997 (EASE97) 2. Comparisons of model concentrations of OH, HO_2, and RO_2 with measurements, *J. Geophys. Res.*, *107*(D14), 4190, doi:10.1029/2001JD001568.

Davis, D., J. Crawford, S. Liu, S. McKeen, A. Bandy, D. Thornton, F. Rowland, D. Blake (1996), Potential impact of iodine on tropospheric levels of ozone and other critical oxidants, *J. Geophys. Res.*, *101*, 2135-2147.

Di Carlo, P. et al. (2004), Missing OH reactivity in a forest: Evidence for unknown reactive biogenic VOCs, *Science*, *304*, 722-725.

Faloona, I. et al. (2001), Nighttime observations of anomalously high levels of hydroxyl radicals above a deciduous forest canopy, *J. Geophys. Res.*, *106*(D20), 24,315–24,334.

Gershenzon, Y. M., V. M. Grigorieva, A. V. Ivanov, and R. G. Remorov (1995), O_3 and OH sensitivity to heterogeneous sinks of HO_x and CH_3O_2 on aerosol particles, *Faraday Discuss.*, *100*, 83-100.

Haggerstone, A.-L., L. J. Carpenter, N. Carslaw, and G. McFiggans (2005), Improved model predictions of HO_2 with gas to particle mass transfer rates calculated using aerosol number size distributions, *J. Geophys. Res.*, *110*, D04303,doi:10.1029/2004JD005282.

Hanson, D. R., J. B. Burkholder, C. J. Howard, and A. R. Ravishankara (1992), Measurement of OH and HO_2 radical uptake coefficients on water and sulfuric acid surfaces, *J. Phys.Chem.*, *96*(12), 4979–4985.

Heard, D. E. and M. J. Pilling (2003), Measurement of OH and HO_2 in the troposphere, *Chem. Rev.*, *103*(12), 5163-5198.

Kanaya, Y., Y. Sadanaga, J. Hirokawa, Y. Kajii, and H. Akimoto, (2001), Development of a ground-based LIF instrument for measuring tropospheric HOx radicals: Instrumentation and calibrations, *J. Atmos. Chem.*, *38*(1), 73-110.

Kanaya, Y., Y. Yokouchi, J. Matsumoto, K. Nakamura, S. Kato, H. Tanimoto, H. Furutani, K. Toyota, and H. Akimoto (2002a), Implications of iodine chemistry for daytime HO_2 levels at Rishiri Island, *Geophys. Res. Lett.*, *29*(8), 1212, doi:10.1029/2001GL014061.

Kanaya, Y., K. Nakamura, S. Kato, J. Matsumoto, H. Tanimoto, and H. Akimoto (2002b), Nighttime variations in HO_2 radical mixing ratios at Rishiri Island observed with elevated monoterpene mixing ratios, *Atmos. Environ.*, *36*(31), 4929-4940.

Kanaya, Y., Y. Kajii and H. Akimoto (2003), Solar actinic flux and photolysis frequency determinations by radiometers and a radiative transfer model at Rishiri Island: comparisons, cloud effects, and detection of an aerosol plume from Russian forest fires, *Atmos. Environ.*, *37*(18), 2463-2475.

Kanaya, Y. and H. Akimoto (2006), Gating a channel photomultiplier using a fast high voltage switch: Reduction of afterpulse rates in a laser-induced fluorescence instrument for measurement of atmospheric OH radical concentrations, *Appl. Opt.*, *45*(6), 1254-1259.

Kato, S., Y. Miyakawa, T. Kaneko, and Y. Kajii (2004), Urban air measurements using PTR/MS in Tokyo

area and comparison with GC-FID measurements, *Int. J. Mass Spectrom.*, *235*(2), 103-110.

Madronich, S. and S. Flocke (1998), The role of solar radiation in atmospheric chemistry, in *Handbook of Environmental Chemistry*, edited by P. Boule, pp. 1-26, Springer-Verlag, New York.

Martinez, M. et al. (2003), OH and HO_2 concentrations, sources, and loss rates during the Southern Oxidants Study in Nashville, Tennessee, summer 1999, *J. Geophys. Res.*, *108*(D19), 4617, doi:10.1029/2003JD003551.

Morita, A., Y. Kanaya, and J. S. Francisco (2004), Uptake of the HO_2 radical by water: Molecular dynamics calculations and their implications for atmospheric modeling, *J. Geophys. Res.*, *109*, D09201, doi:10.1029/2003JD004240.

Mozurkewich, M., P. H. McMurry, A. Gupta, and J. G. Calvert (1987), Mass accommodation coefficient of HO_2 radicals on aqueous particles, *J. Geophys. Res.*, *92*(D4), 4163–4170.

Ravishankara, A. R., E. J. Dunlea, M. A. Blitz, T. J. Dillon, D. E. Heard, M. J. Pilling, R. S. Strekowski, J. M. Nicovich, and P. H. Wine (2002), Redetermination of the rate coefficient for the reaction of $O(^1D)$ with N_2, *Geophys. Res. Lett.*, *29*(15), 1745, doi:10.1029/2002GL014850.

Ren, X. et al. (2003), OH and HO_2 Chemistry in the urban atmosphere of New York City, *Atmos. Environ.*, *37*(26), 3639–3651.

Saiz-Lopez, A., and J. M. C. Plane (2004), Novel iodine chemistry in the marine boundary layer, *Geophys. Res. Lett.*, *31*, L04112, doi:10.1029/2003GL019215.

Salisbury, G. et al. (2001), Production of peroxy radicals at night via reactions of ozone and the nitrate radical in the marine boundary layer, *J. Geophys. Res.*, *106*(D12), 12,669–12,688.

Sander, S. P. et al. (2003), Chemical kinetics and photochemical data for use in stratospheric modeling, evaluation number 14, *JPL Publ. 02– 25*, NASA Jet Propul. Lab., Pasadena, Calif.

Sommariva, R., A. -L. Haggerstone, L. J. Carpenter, N. Carslaw, D. J. Creasey, D. E. Heard, J. D. Lee, A. C. Lewis, M. J. Pilling, J. Zádor (2004), OH and HO_2 chemistry in clean marine air during SOAPEX-2, *Atmos. Chem. Phys.*, *4*, 839-856.

Sommariva, R. et al. (2006), OH and HO_2 chemistry during NAMBLEX: roles of oxygenates, halogen oxides and heterogeneous uptake, *Atmos. Chem. Phys. 6,* 1135-1153.

Stockwell, W. R., F. Kirchner, M. Kuhn, and S. Seefeld (1997), A new mechanism for regional atmospheric chemistry modeling, *J. Geophys. Res.*, *102*(D22), 25,847–25,880.

Stutz, J., K. Hebestreit, B. Alicke, and U. Platt (1999), Chemistry of halogen oxides in the troposphere: Comparison of model calculations with recent field data, *J. Atmos. Chem*., *34*, 65-85.

Tanimoto, H., O. Wild, S. Kato, H. Furutani, Y. Makide, Y. Komazaki, S. Hashimoto, S. Tanaka, and H. Akimoto (2002), Seasonal cycles of ozone and oxidized nitrogen species in northeast Asia 2. A model analysis of the roles of chemistry and transport, *J. Geophys. Res*., *107*(D23), 4706, doi:10.1029/2001JD001497.

Tanner, D. et al. (2002), Measurement and model results for gas phase OH and H_2SO_4 during PROPHET 2001, *Eos Trans. AGU*, *83*(47), Fall Meet. Suppl., Abstract A51A-0037.

Vogt, R., R. Sander, R. von Glasow, and P. J. Crutzen (1999), Iodine chemistry and its role in halogen activation and ozone loss in the marine boundary layer: A model study, *J. Atmos. Chem*., *32*, 375-395.

Yienger, J. and H. Levy (1995), Empirical model of global soil-biogenic NOx emissions, *J. Geophys. Res*., *100*(D6), 11,447–11,464.

Yokouchi, Y. et al. (2005), Correlations and emission ratios among bromoform, dibromochloromethane, and dibromomethane in the atmosphere, *J. Geophys. Res.*, *110*, D23309, doi:10.1029/2005JD006303.

Figure captions

Figure 1. Temporal variations in (a) HO_2 and (b) OH concentrations. Observed data (10-min averages) are shown by solid circles. Those data modeled using RACM (with monoterpene chemistry) are shown by gray lines. Modeled HO_2 levels with heterogeneous loss of HO_2 on aerosol surfaces (red lines) and those with higher reaction rate coefficients for the $HO_2 + RO_2$ reactions (blue lines) are also shown in (a). In (b), OH levels estimated from the observed HO_2 levels are shown by green + symbols.

Figure 2. Composite diurnal variations in observed (a) HO_2 and (b) OH concentrations at Rishiri Island for September 2003. The 1-min data are shown by small open gray circles, while hourly averages (and 1σ range) are shown by large gray circles with error bars.

Figure 3. Scatterplots of observed and modeled (a) HO_2 mixing ratios and (b) OH concentrations. Only daytime (0900–1500 LST) data are used.

Figure 4. Modeled-to-observed (a) HO_2 and (b) OH ratios plotted as functions of the NO mixing ratio. Ten-minute averaged data in the daytime (0900–1500 LST) are used. The vertical gray bars indicate uncertainties in the ratios calculated from variations in observed 1-min concentrations included in the 10-min period.

Figure 5. Loss rate of HO_2 (k) required to reduce the calculated HO_2 levels to observed levels (+ symbols). The maximum possible loss rate of HO_2 due to heterogeneous loss on aerosol surfaces is shown by a gray line.

Figure 6. Composite diurnal variations in the missing loss rate of HO_2 (k) for September 2003 (open circles) compared to that for June 2000 (gray circles).

Figure 7. Breakdown of the production and loss processes of HO_2, OH and the radical group ($OH+HO_2+RO_2$). Daytime median values (0900–1500 LST) in the base run are used. Species in the model are isoprene (ISO), peroxy radicals formed from ISO and dienes (ISOP), acetaldehyde and higher aldehydes (ALD), methylglyoxal and other α-carbonyl aldehydes (MGLY), methacrolein and other unsaturated monoaldehydes (MACR), unsaturated dicarbonyls (DCB), parametric peroxy radicals that account for additional NO to NO_2 conversions (XO_2), peroxy radicals formed from alkanes, alcohols, esters, and alkynes with OH rate constant (298 K, 1 atm) less than 3.4×10^{-12} cm^3 s^{-1} (HC3P), and peroxy radicals formed from terminal alkenes (OLTP).

Figure 8. Total monoterpene concentrations measured using PTR-MS (10-min averages: gray line; 1-hour averages: + symbols) compared with the summed concentrations of four monoterpene species (α-pinene, β-pinene, camphene, and limonene) measured using GC-MS (open squares). Vertical gray bars represent the nights (21–22, 25–26, and 27–28 September) for which continuous OH and HO_2 measurements were performed.

Figure 9. Observed nighttime HO_2 concentrations plotted against (a) total monoterpene concentrations, (b) radical production rate from the ozonolysis of four monoterpenes, and (c) ozone concentrations. All data points are 10-min averages. Data for 21–22 September: circles; 25–26 September: triangles; 27–28 September: squares; nighttime data other than the three nights listed previously: diamonds. (d)–(f) Same plots but for observed nighttime OH concentrations (using 1-hour averages).

Figure 10. Temporal variations in observed (red circles) and modeled (solid lines) HO_2 and OH concentrations for the three analyzed nights. Red, orange (only in HO_2 plots), yellow, green (in both HO_2 and OH plots), light blue, and blue lines (only in OH plots) correspond to model runs with fixed NO concentrations of 1, 2, 5, 10, 20, and 50 pptv, respectively. The black dashed line for HO_2 on 25–26 September (b) shows the model results where OH concentrations were constrained to the observed 10-min values. The total monoterpene concentrations are shown by shaded bars in the HO_2 plots. The black circles in the OH plots represent 10-min averages. The error bars of the observed hourly OH levels show the 1-σ range for 10-min values included in the hourly data.

Figure 11. Dependence of observed (open symbols) and modeled (gray symbols) nighttime (a) HO_2

mixing ratios on square root of radical production rate and (b) OH concentrations on radical production rate. Modeled levels are those for 5 pptv NO. Data for 21–22, 25–26, and 27–28 September are shown by circles, triangles, and squares, respectively. The error bars indicate the 1-σ range for 1-min (for HO_2) or 10-min (for OH) values in the 10-min (for HO_2) or hourly (for OH) data.

Figure 12. Breakdown of the production and loss processes of HO_2, OH, and the radical group ($OH+HO_2+RO_2$) at selected times during the night. A value of 5 pptv of NO was assumed in the model run. Species in the model are terminal alkenes (OLT), internal alkenes (OLI), α-pinene (API), β-pinene (BPI), camphene (CMP), limonene (LIM), peroxy radical formed from ethane (ETHP), peroxy radical formed from ketones (KETP), NO_3-alkene adduct reacting via decomposition (OLND), peroxy radical formed from α-pinene (APIP), peroxy radical formed from β-pinene (BPIP), peroxy radical formed from camphene (CMPP), and peroxy radical formed from limonene (LIMP).

Table 1. Chemical Species and Parameters Observed During the Campaign

Chemical species/meteorol. parameter	Method
O_3	UV absorption
CO	nondispersive infrared spectroscopy
OH, HO_2	laser-induced fluorescence (LIF)
Non-methane hydrocarbons	gas chromatography/flame ionization detector
Non-methane hydrocarbons	gas chromatography/mass spectrometry
NO, NO_2	Xe lamp photolytic conversion/chemiluminescence
PANs	gas chromatography/mass spectrometry
HO_2+RO_2	chemical amplification/luminol NO_2 detection
HO_2+RO_2	chemical amplification/LIF NO_2 detection
DMS, CH_3CN, non-methane hydrocarbons, OVOC	proton transfer reaction- mass spectrometry
Organoiodines, DMS	gas chromatograph/mass spectrometry
SO_2	pulsed fluorescence
Na^+, NH_4^+, K^+, Ca^{2+}, Mg^{2+}, Cl^-, NO_3^-, SO_4^{2-}/aerosol	filter/ion chromatography
Trace metal/ aerosol	filter/ inductively coupled plasma mass spectrometer
Organic carbon / aerosol	micro-orifice uniform-deposit impactor
Black carbon	absorption photometry
Fine particle (0.1 – >0.5 um) number density	optical particle counter
4.5–163 nm particle number density	scanning mobility particle sizer
T, RH (H_2O), atmospheric pressure, wind	
$J(NO_2)$	filter radiometer
Spectral actinic flux, other *J* values	spectroradiometer

Table 2. Chemical Species and Meteorological Parameters with High Correlation Coefficients (R) with the Loss Rate of HO_2 (k) that are Required to Reduce the Modeled HO_2 Levels to the Observed Levels

species/parameter		R
O^1D	modeled	0.72
J values	measured	0.68–0.71
RO_2	modeled	0.34–0.69
transmission factor	measured	0.49
HCHO	assumed	0.49
HO_2	measured	0.48
CSL (cresol etc.)	modeled	0.46
OH	measured	0.45
wind speed (m/s)	measured	0.42
CH_3COOOH	modeled	0.41
$CHBr_3$	measured	0.35
temperature	measured	0.34
GLY (glyoxal etc.)	modeled	0.33
CO	measured	0.32
CH_3I	measured	0.31
CH_3Cl	measured	0.30
-(tidal height)	reported	0.27
H_2O	measured	0.22
particles (300–500 nm)	measured	0.22

Table 3. Average Nighttime Values of OH, HO_2, and Ancillary Measurements

1800–0459 LST average	Sep. 21–22	Sep. 25–26	Sep. 27–28
OH (10^5 cm^{-3})	1.6 ± 0.5	3.4 ± 1.2	1.6 ± 0.5
(number of 60-min data)	(11)	(11)	(11)
HO_2 (pptv)	1.3 ± 0.2	2.6 ± 0.9	0.7 ± 0.2
(number of 10-min data)	(62)	(53)	(63)
NO (pptv)	4.1	6.3	5.8
NO_2 (pptv)	145	382	90
O_3 (ppbv)	24.9	19.8	35.4
modeled[a] NO_3 (pptv)	0.17	0.09	0.27
Σmonoterpene (pptv)	105	366	21
Temperature (K)	285.0	288.6	285.7
RH (%)	67	94	86
Wind direction (degree)	344	33	79
Wind speed (m s^{-1})	2.0	0.8	4.0

[a]modeled with 5 pptv of NO

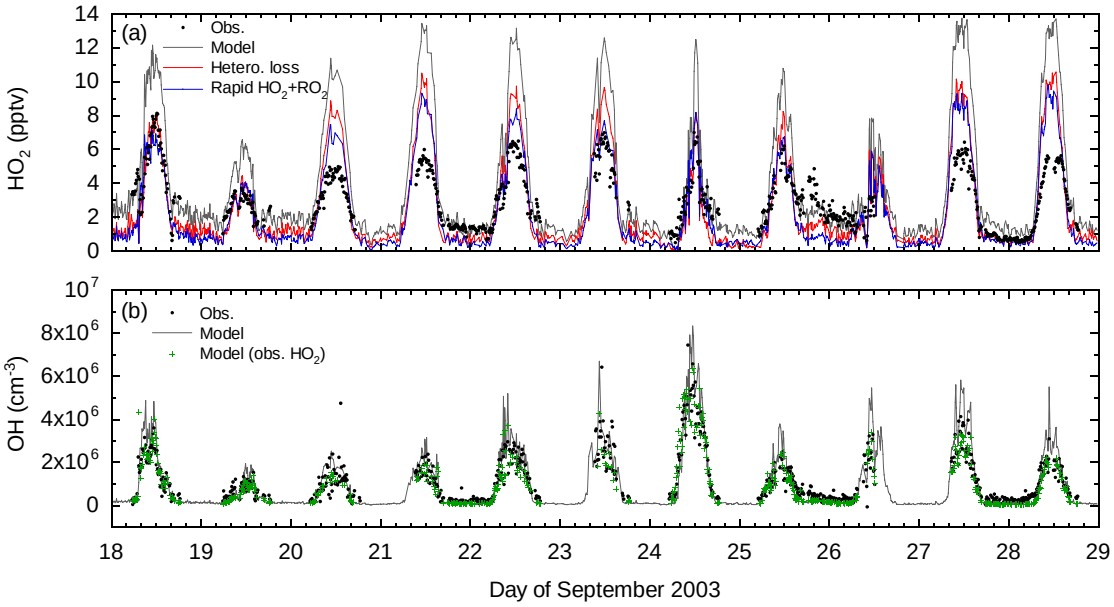

Figure 1. Temporal variations in (a) HO_2 and (b) OH concentrations. Observed data (10-min averages) are shown by solid circles. Those data modeled using RACM (with monoterpene chemistry) are shown by gray lines. Modeled HO_2 levels with heterogeneous loss of HO_2 on aerosol surfaces (red lines) and those with higher reaction rate coefficients for the HO_2 + RO_2 reactions (blue lines) are also shown in (a). In (b), OH levels estimated from the observed HO_2 levels are shown by green + symbols.

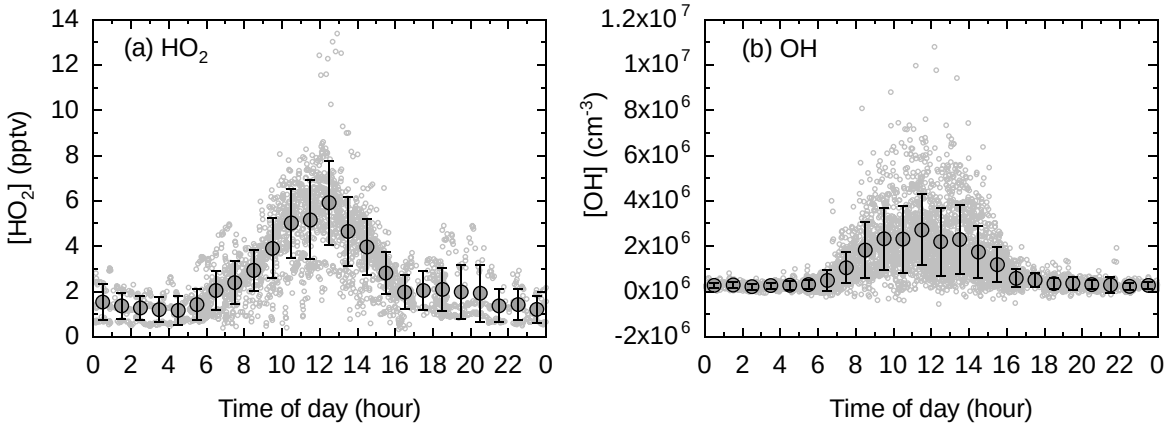

Figure 2. Composite diurnal variations in observed (a) HO_2 and (b) OH concentrations at Rishiri Island for September 2003. The 1-min data are shown by small open gray circles, while hourly averages (and 1σ range) are shown by large gray circles with error bars.

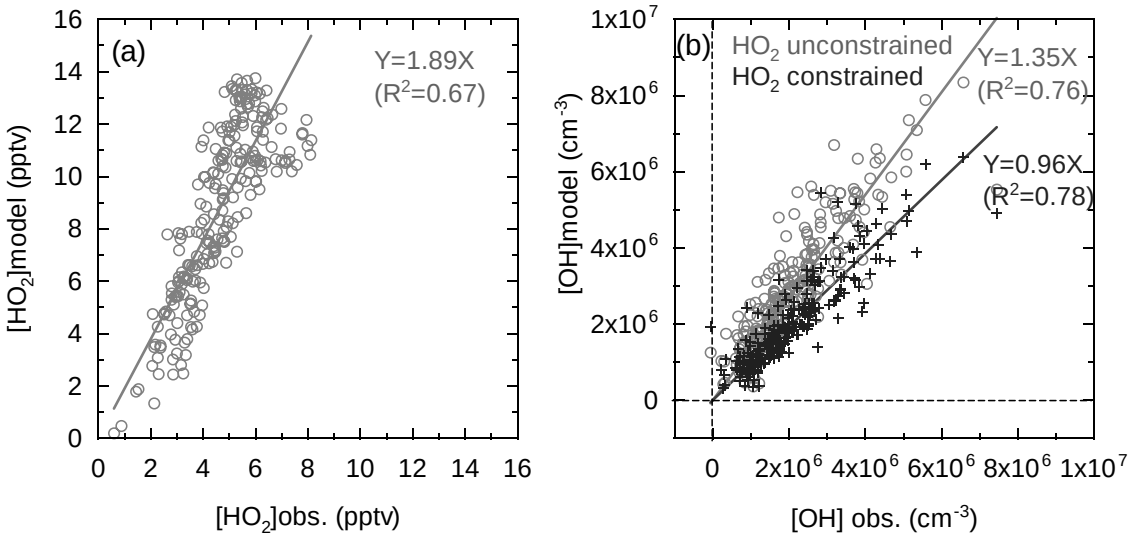

Figure 3. Scatterplots of observed and modeled (a) HO_2 mixing ratios and (b) OH concentrations. Only daytime (0900–1500 LST) data are used.

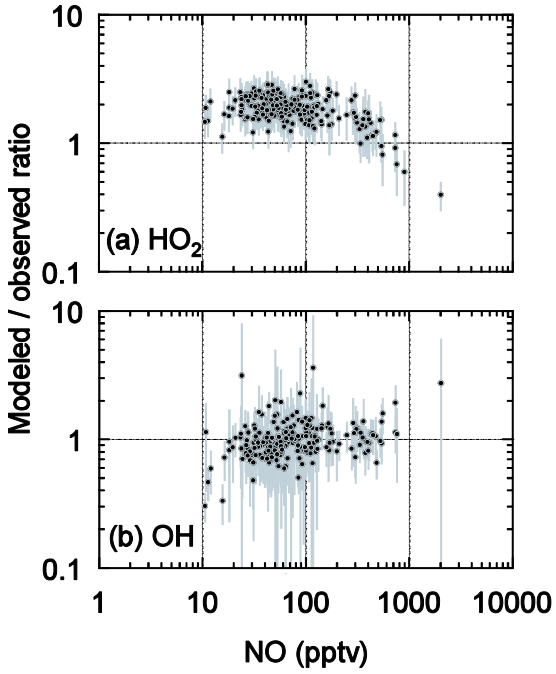

Figure 4. Modeled-to-observed (a) HO_2 and (b) OH ratios plotted as functions of the NO mixing ratio. Ten-minute averaged data in the daytime (0900–1500 LST) are used. The vertical gray bars indicate uncertainties in the ratios calculated from variations in observed 1-min concentrations included in the 10-min period.

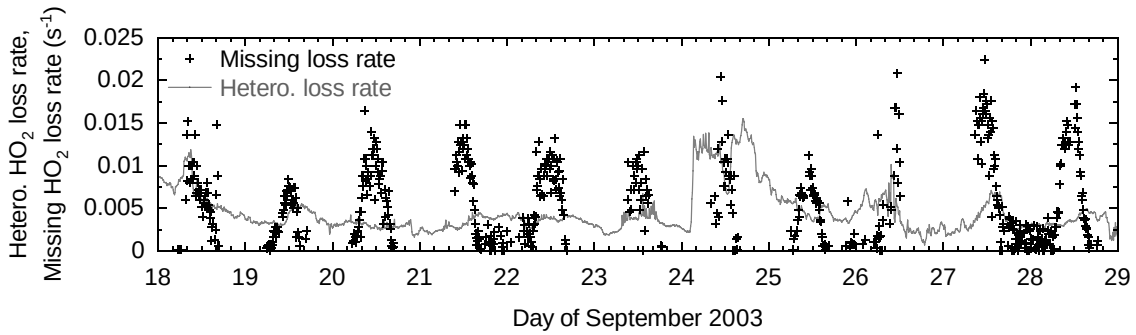

Figure 5. Loss rate of HO_2 (k) required to reduce the calculated HO_2 levels to observed levels (+ symbols). The maximum possible loss rate of HO_2 due to heterogeneous loss on aerosol surfaces is shown by a gray line.

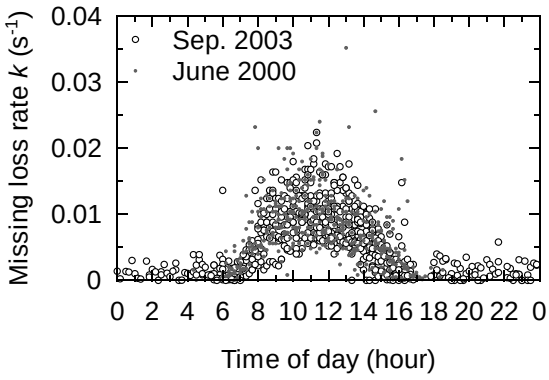

Figure 6. Composite diurnal variations in the missing loss rate of HO_2 (k) for September 2003 (open circles) compared to that for June 2000 (gray circles).

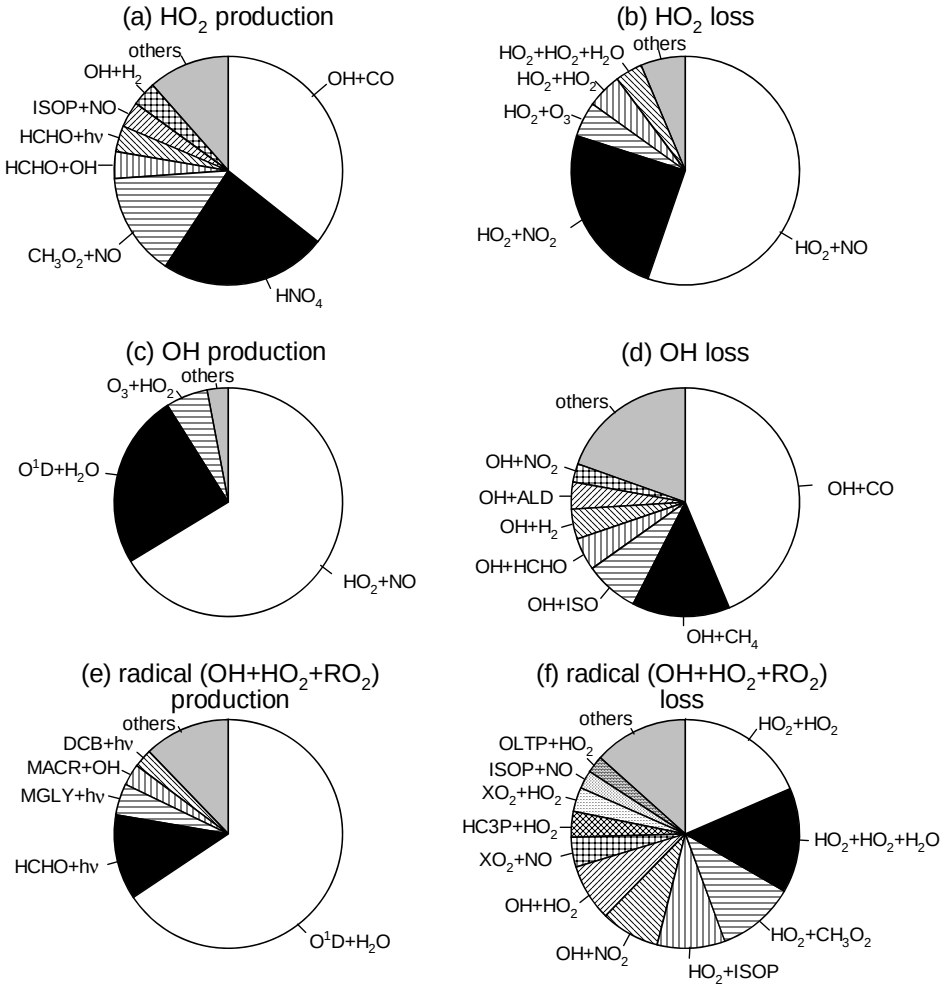

Figure 7. Breakdown of the production and loss processes of HO_2, OH and the radical group ($OH+HO_2+RO_2$). Daytime median values (0900–1500 LST) in the base run are used. Species in the model are isoprene (ISO), peroxy radicals formed from ISO and dienes (ISOP), acetaldehyde and higher aldehydes (ALD), methylglyoxal and other α-carbonyl aldehydes (MGLY), methacrolein and other unsaturated monoaldehydes (MACR), unsaturated dicarbonyls (DCB), parametric peroxy radicals that account for additional NO to NO_2 conversions (XO_2), peroxy radicals formed from alkanes, alcohols, esters, and alkynes with OH rate constant (298 K, 1 atm) less than 3.4×10^{-12} cm^3 s^{-1} (HC3P), and peroxy radicals formed from terminal alkenes (OLTP).

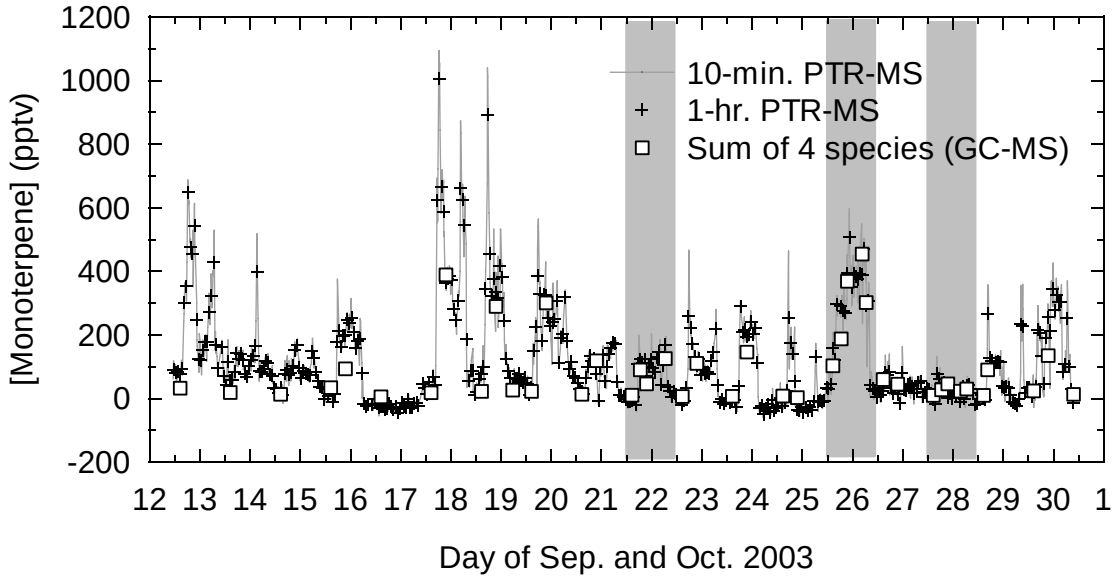

Figure 8. Total monoterpene concentrations measured using PTR-MS (10-min averages: gray line; 1-hour averages: + symbols) compared with the summed concentrations of four monoterpene species (α-pinene, β-pinene, camphene, and limonene) measured using GC-MS (open squares). Vertical gray bars represent the nights (21–22, 25–26, and 27–28 September) for which continuous OH and HO_2 measurements were performed.

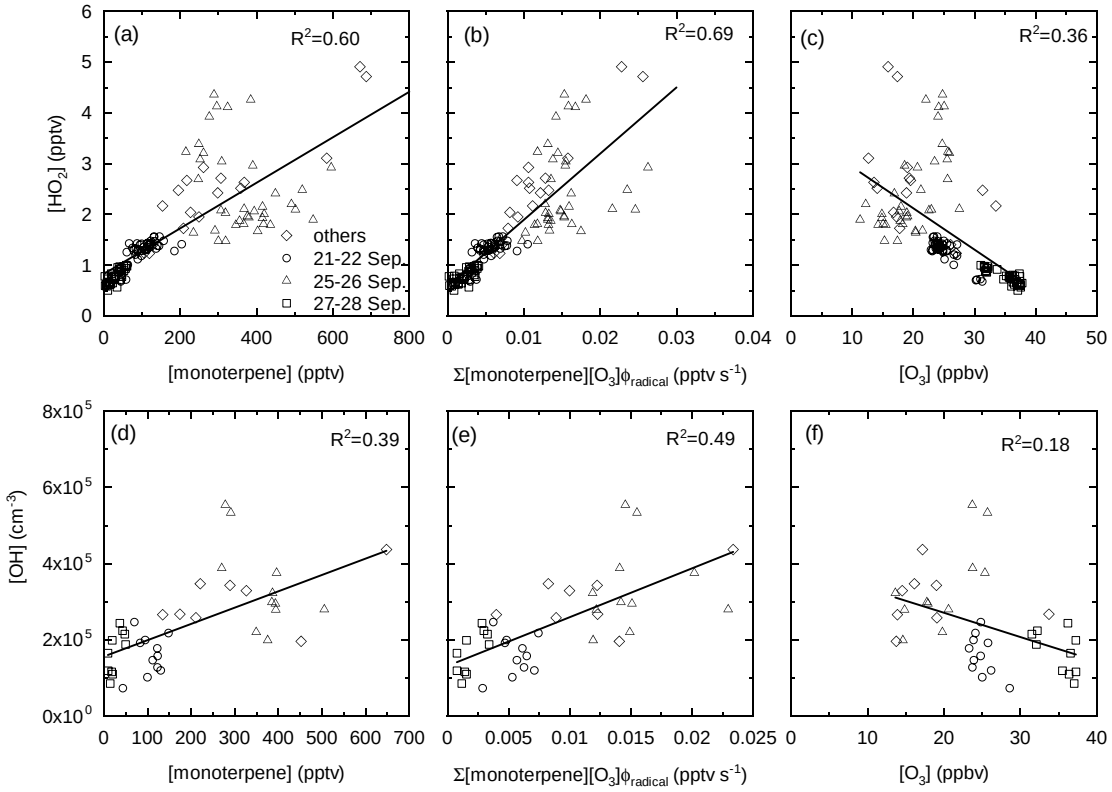

Figure 9. Observed nighttime HO_2 concentrations plotted against (a) total monoterpene concentrations, (b) radical production rate from the ozonolysis of four monoterpenes, and (c) ozone concentrations. All data points are 10-min averages. Data for 21–22 September: circles; 25–26 September: triangles; 27–28 September: squares; nighttime data other than the three nights listed previously: diamonds. (d)–(f) Same plots but for observed nighttime OH concentrations (using 1-hour averages).

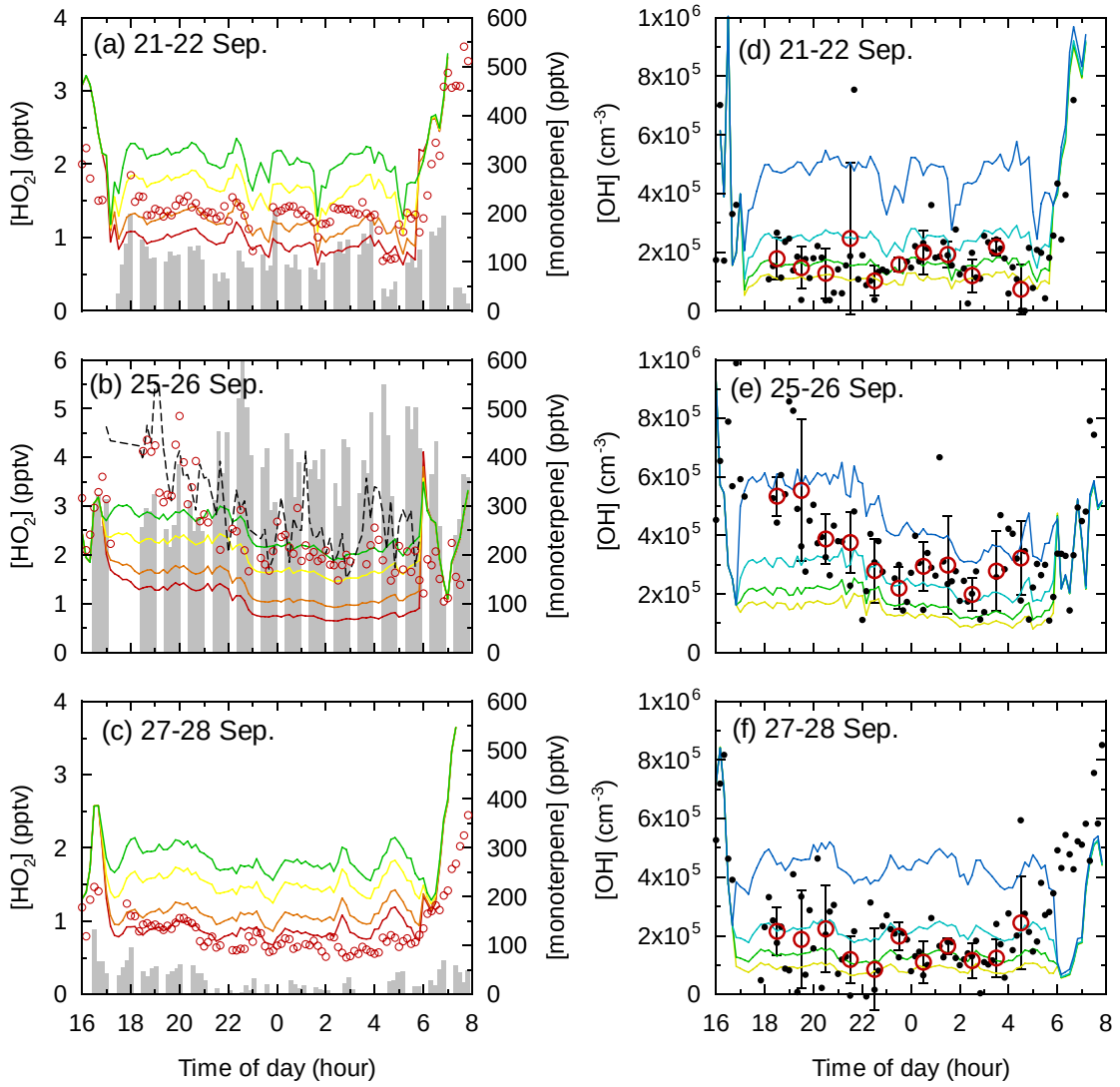

Figure 10. Temporal variations in observed (red circles) and modeled (solid lines) HO_2 and OH concentrations for the three analyzed nights. Red, orange (only in HO_2 plots), yellow, green (in both HO_2 and OH plots), light blue, and blue lines (only in OH plots) correspond to model runs with fixed NO concentrations of 1, 2, 5, 10, 20, and 50 pptv, respectively. The black dashed line for HO_2 on 25–26 September (b) shows the model results where OH concentrations were constrained to the observed 10-min values. The total monoterpene concentrations are shown by shaded bars in the HO_2 plots. The black circles in the OH plots represent 10-min averages. The error bars of the observed hourly OH levels show the 1-σ range for 10-min values included in the hourly data.

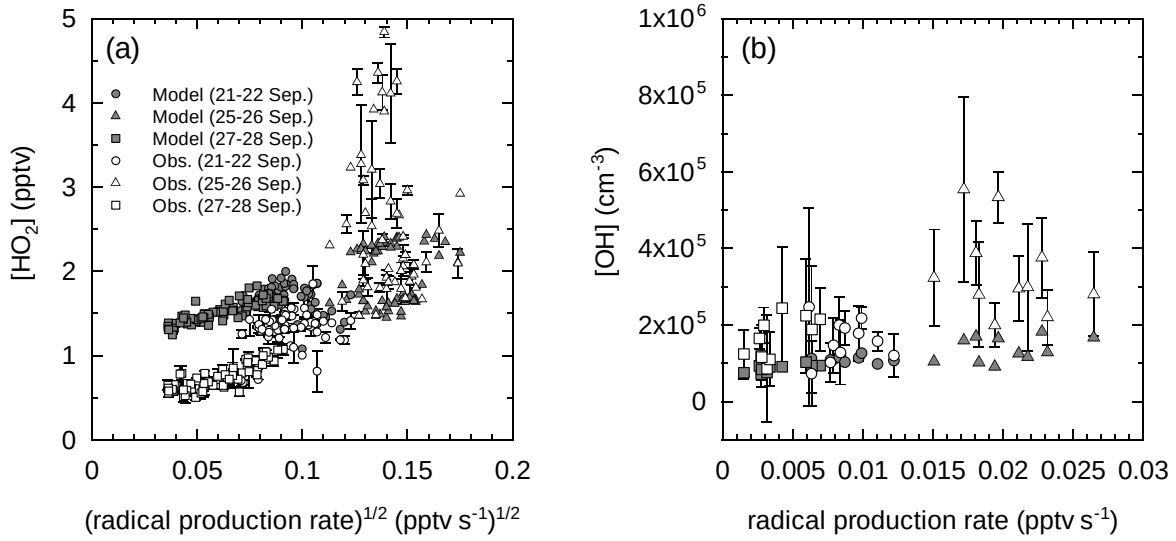

Figure 11. Dependence of observed (open symbols) and modeled (gray symbols) nighttime (a) HO_2 mixing ratios on square root of radical production rate and (b) OH concentrations on radical production rate. Modeled levels are those for 5 pptv NO. Data for 21–22, 25–26, and 27–28 September are shown by circles, triangles, and squares, respectively. The error bars indicate the 1-σ range for 1-min (for HO_2) or 10-min (for OH) values in the 10-min (for HO_2) or hourly (for OH) data.

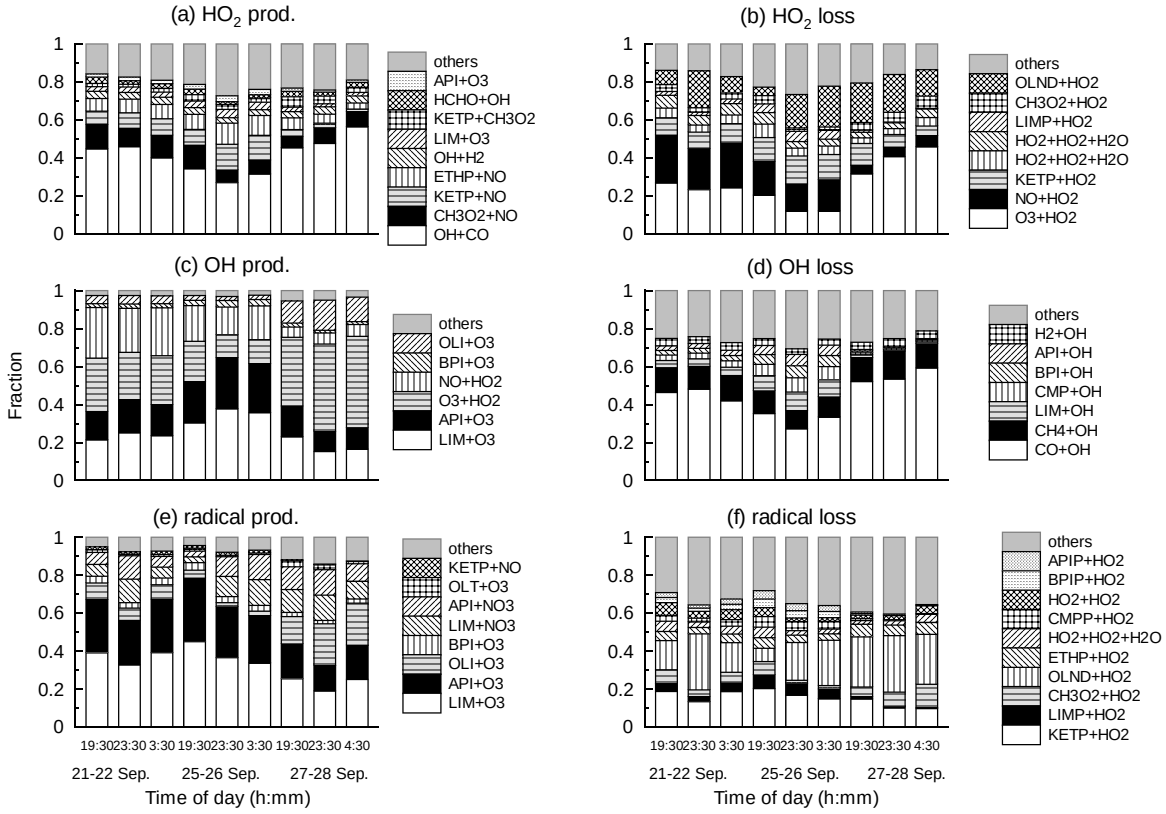

Figure 12. Breakdown of the production and loss processes of HO_2, OH, and the radical group ($OH+HO_2+RO_2$) at selected times during the night. A value of 5 pptv of NO was assumed in the model run. Species in the model are terminal alkenes (OLT), internal alkenes (OLI), α-pinene (API), β-pinene (BPI), camphene (CMP), limonene (LIM), peroxy radical formed from ethane (ETHP), peroxy radical formed from ketones (KETP), NO_3-alkene adduct reacting via decomposition (OLND), peroxy radical formed from α-pinene (APIP), peroxy radical formed from β-pinene (BPIP), peroxy radical formed from camphene (CMPP), and peroxy radical formed from limonene (LIMP).